

Geometrical model-based segmentation of the organs of sight on CT images

György Bekes^{a)}

Healthcare Division, GE Hungary ZRt., Szikra u. 2, H-6725 Szeged, Hungary

Eörs Máté, László G. Nyúl, and Attila Kuba

Department of Image Processing and Computer Graphics, University of Szeged, Árpád ter 2., H-6720 Szeged, Hungary

Márta Fidrich

Healthcare Division, GE Hungary ZRt., Szikra u. 2, Szeged, Hungary

(Received 27 October 2006; revised 24 October 2007; accepted for publication 19 November 2007; published 29 January 2008)

Segmentation of organs of sight such as the eyeballs, lenses, and optic nerves is a time consuming task for clinicians. The small size of the organs and the similar density of the surrounding tissues make the segmentation difficult. We developed a new algorithm to segment these organs with minimal user interaction. The algorithm needs only three seed points to fit an initial geometrical model to start an effective segmentation. The clinical evaluation shows that the output of our method is useful in clinical practice. © 2008 American Association of Physicists in Medicine. [DOI: [10.1118/1.2826557](https://doi.org/10.1118/1.2826557)]

Key words: radiotherapy, CT imaging, image segmentation, geometrical model

I. INTRODUCTION

In radiotherapy planning, clinicians (radiologists, dosimetrists, or radiotherapists) have to determine the outline of certain organs on a large number of images. Manually drawing the individual contours on a contiguous set of two-dimensional (2D) slices is very time consuming and labor intensive. The time and labor increase with the number of image slices, and the number and sizes of the organs, tumors, etc., in the anatomical volume of interest. The quality of the three-dimensional segmentation highly depends on the resolution and contrast of the 2D images as well as on the experience of the clinician. The use of automated image segmentation can save effort and can also increase precision by eliminating the subjectivity of the clinician. There are several regions of interest in radiation treatment planning that can be either targets (e.g., a tumor) or regions that should be avoided. The organs of sight—eyeballs, lenses and nerves—are very sensitive to radiation, and thus should be avoided during the treatment.

II. RELATED WORKS

Several published methods exist for the segmentation of organs of sight. These are usually some variants of deformable model-based methods and work on magnetic resonance (MR) on visible human project (VHP) images. The model-based segmentation technique combines information of three-dimensional (3D) image and anatomical information. The model is adapted to the 3D image by some deformation.

The method of Dobler and Bendl¹ builds a precise geometric model of the eye for proton therapy, using ellipsoid and cylindrical shapes for the different parts of the ocular system. Parameters for most objects are set via ultrasound measurements, and the rest is set to predetermined fixed val-

ues. The geometric model is adapted to the particular image volume using atlas-based image registration. In their model, the eyeball is an ellipsoid with variable length half axes, and the lens is defined as the intersection of two ellipsoids. In contrast, we simplify the eyeball to a sphere and our lens model is a single ellipsoid. The optic nerve is not considered by Dobler and Bendl as a main target and therefore its segmentation is not fully explored, only a small cylinder is used to model its base emerging from the eye. Our method segments the entire segment of the nerve up to the optic chiasm.

Souza and Ruiz² gave an algorithm to detect the extraocular muscle border (EOM). It is based on the fact that EOM has elliptic or circular pattern and it has higher intensities than the surrounding structures. The segmentation is performed using morphological operators and the Laplacian of Gaussian as edge detector. We also use elliptic approximation for the optic nerve, which seems natural considering the similar shape of the EOM and the optic nerve. Other structures of the eye are not segmented in Ref. 2.

In the work of Kaus *et al.*³ the model is represented by a triangular mesh. It is positioned by the user interactively using scaling and rotating tools. The triangular surface mesh is then adapted to the image by iterative optimization. This method can be used mostly to segment bigger organs. In our case, seven relatively small structure must be segmented and manual positioning of the individual models would be very time-consuming and inaccurate. Unfortunately, automatic registration of the model is not reliable because of the lack of good landmarks.

The method of D'Haese *et al.*⁴ segments the organs of sight and some brain structures by applying predefined anatomical models that are deformed to get the result. The method is performed on MR images, where the contrast is

better and separation of different tissue types is easier, compared to our computed tomography (CT) images.

Cates *et al.*⁵ give an evaluation for watershed segmentation of brain VHP studies. The contour of the different structures can be well observed on VHP data, therefore the segmentation is easier than in our case, where usually diagnostic quality CT images are used.

Unfortunately, none of the currently available methods fulfills all of our requirements, therefore we devised a new algorithm that combines anatomical knowledge and modeling. The method presented here segments the organs of sight using a model that is created on the fly from simple geometrical shapes and positioned with three seed points specified by the user. In our case, the key points are quick computation and minimal user interaction. The precision of the segmentation is less important, because the input images have various resolution and a margin is applied (according to the radiotherapy planning protocol) around the segmented region to avoid them during the treatment.

In Sec. III we give a short anatomical background of our segmentation task. Sec. IV explains how our model is built, while details for the individual components applied to the CT images are given in Sec. V. Section VI describes our evaluation method and we show and discuss the results in Sec. VII.

III. ANATOMICAL BACKGROUND

The *eyeball* is contained in the cavity of the orbit. The eyeball is embedded in the fat of the orbit, but it is separated from it by a thin membranous sac. Segmentation of the eyeball is relatively easy, because the density of the eyeball differs from the surrounding tissues and the boundary of the eyeball is well visible.

The *crystalline lens* is a transparent optical element that serves to change the degree of convergence or divergence of the transmitted rays. It is situated behind the iris in the eye. It can be seen well, because its density differs from the surrounding organs, such as the aqueous humour and vitreous humour. Aqueous humour is a clear, watery fluid circulating in the chamber of the eye between the cornea and the lens. Vitreous humour is a transparent jellylike substance behind the lens of the vertebrate eye. Vitreous humour gives rigidity to the spherical form of the eye and allows light to pass through to the retina.

The *optic nerve* is a continuation of the axons of the ganglion cells in the retina. It acts like a cable connecting the eye with the brain and actually it is more like brain tissue than nerve tissue. As the optic nerve leaves the back of the eye, it travels to the optic chiasm, located just below and in front of the pituitary gland. It is embedded into tetrobulbar connective tissue, so it can be seen well, but the nerve shears, hence the segmentation is difficult.

The *optic chiasm* is the crossing of the optic nerves from the two eyes at the base of the brain. Delineation of this organ is very difficult due to its small size and because its intensity values cannot be separated from its environment, such as nerve and brain tissue. The crossing's height can

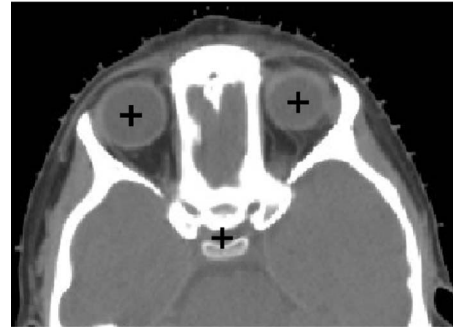


FIG. 1. Seed points indicating the centers of the eyeballs and the optic chiasm.

only be benchmarked against the foramen optimum. The extension of the optic chiasm cannot be known due to similar densities. Therefore, the manual segmentation of the shape of the optic chiasm is also very difficult.

IV. MODELING

Based on some 3D anatomical atlas and discussion with clinicians we found that these organs can be effectively modeled with simple geometrical shapes. The eyeball is very similar to a sphere and the lens is like an ellipsoid. The eyeball may have ellipsoid shapes, but in our image (because of their resolution) it cannot be detected, and this difference can be compensated with a margin. The muscles (connected to the eyeball) and the optic nerve among them have a conical shape, and the optic canal is like a cylinder.

Usually, applying a model means that it has to be positioned and deformed to match the image data either manually or with some registration method. In our case, there are seven objects to be segmented that have relatively small size. The delineation of the nerves is especially difficult on axial slices. Manual positioning (including scaling and rotation) is very difficult and registration is too complex without reliable landmarks. Therefore, we construct our model on the fly from the above mentioned primitives, which are positioned and scaled with the help of the three seed points specified by the user and adapted to the resolution of the input image. The inspiration came from the constructive solid geometry,⁶ which allows the modeler to create complex, hierarchical object description by using Boolean operators, translation, rotation, and scaling to combine primitives.

V. METHOD DETAILS

The user is required to select three points (see Fig. 1), which may be given on different slices. Two of these points should be in the center of each eyeball and the third seed point should be in the optic nerve. The order of the segmentation of the different objects is the following:

1. Eyeballs: approximated with spheres. The given seed points are used to help the thresholding of these organs.
2. Lenses: approximated with ellipsoids inside the eyeballs.
3. Optic nerves: approximated from two directions. They are modeled with a cone and cylinder.

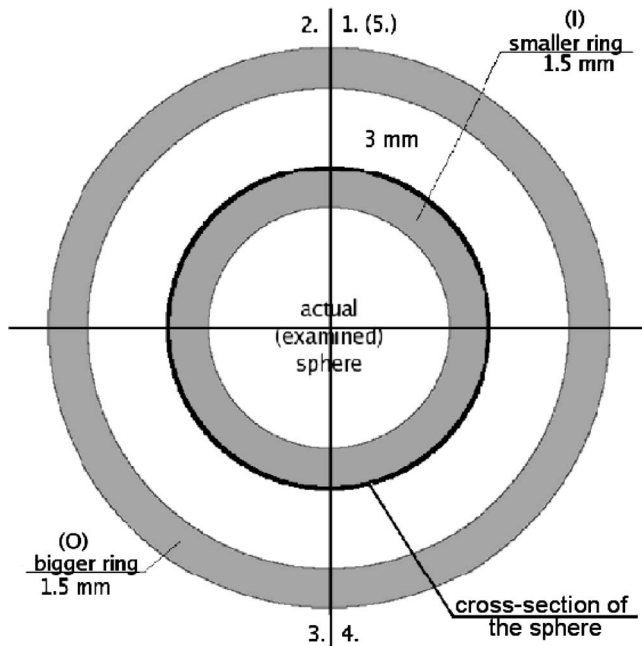


FIG. 2. Two-dimensional cross-section of the two spherical shells used for computing the goodness of fit. Only the voxels in the shaded area are used for computation.

4. Optic chiasm: modeled with a predefined shape.

The algorithm has many parameters and these were set during an experimental cycle using a set of “training” images.

V.A. Segmentation of the eyeballs

The eyeball is segmented by fitting a sphere to the image data suitably. In order to find the best fit for the eyeball the following properties are used: inside the eyeball (including the lens) the CT values are between 0 and 110 Hounsfield Units (HU), its environment has intensity usually under -20 HU or above 150 HU. Furthermore, we suppose that the user given seed point is near the center of the eyeball.

Let $S(\mathbf{P}, r)$ denote the sphere having center $\mathbf{P}=(x, y, z)$ and radius r . Then let

$$I(\mathbf{P}, r) = S(\mathbf{P}, r) \setminus S(\mathbf{P}, r - 1.5 \text{ cm}) \text{ and} \quad (1)$$

$$O(\mathbf{P}, r) = S(\mathbf{P}, r + 4.5 \text{ cm}) \setminus S(\mathbf{P}, r + 3 \text{ cm}) \quad (2)$$

define two 3D spherical shells (see Fig. 2) that are used during the search. These shells must be fitted so that I is inside and O is outside the eyeball. The best fit is found by optimization, that is, by finding the minimum of a cost function defined in a parameter space of \mathbf{P} and r where the voxel size is taken into account. The cost function $C(\mathbf{P}, r)$ uses a soft classification of voxels based on their HU values (see Fig. 3). For computational efficiency, it only considers voxels that are in the intersection of the two spherical shells (see Fig. 2) and the three planes of the main directions (axial, coronal and sagittal) passing through the center of the ball. The solution (\mathbf{P}_e, r_e) is found by a four-level coarse-to-fine search, wherein at each level, the finer search is performed in the vicinity of the optima found at the preceding coarser scale (see Algorithm 1). The optimization here means calculating the value of the cost function at discrete points of the parameter space and taking their minima.

Algorithm 1 Fitting of the sphere

- 1: $\mathbf{P}_e :=$ the given eyeball seed point (x_e, y_e, z_e)
- 2: $r_e :=$ the radius of an average eyeball
- 3: $optval := +\infty$
- 4: **for** Level=0 to 3 **do**
- 5: $(\mathbf{P}_o, r_o) := \arg \min_{\substack{|x-x_e| \leq d_x \\ |y-y_e| \leq d_y \\ |z-z_e| \leq d_z \\ |r-r_e| \leq d_r}} C(\mathbf{P}, r)$
- 6: **if** $C(\mathbf{P}_o, r_o) < optval$ **then**
- 7: $(\mathbf{P}_e, r_e) := (\mathbf{P}_o, r_o)$
- 8: $optval := C(\mathbf{P}_o, r_o)$
- 9: **end if**
- 10: Decrease d_x, d_y, d_z, d_r
- 11: **end for**

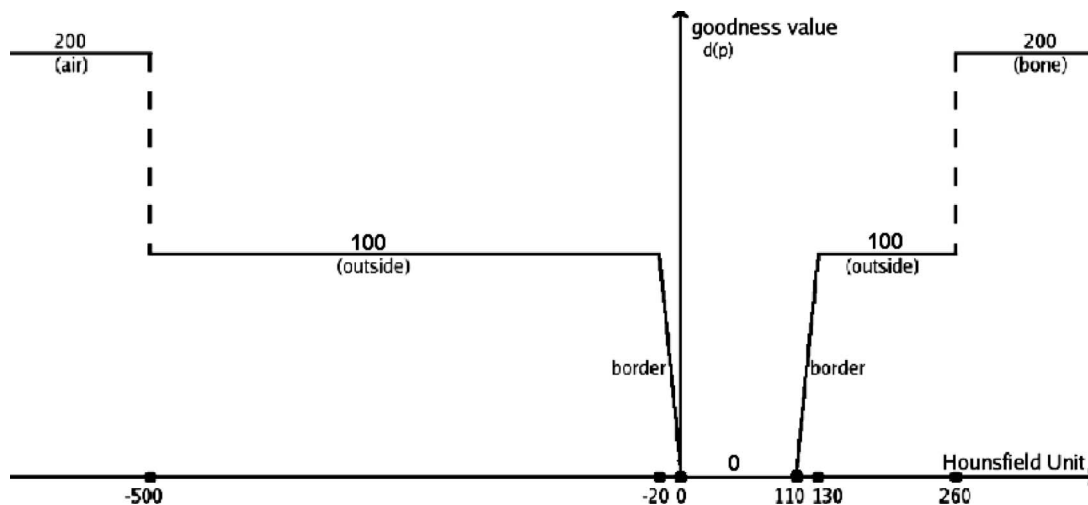


FIG. 3. Soft classification of the voxels based on the HU values.

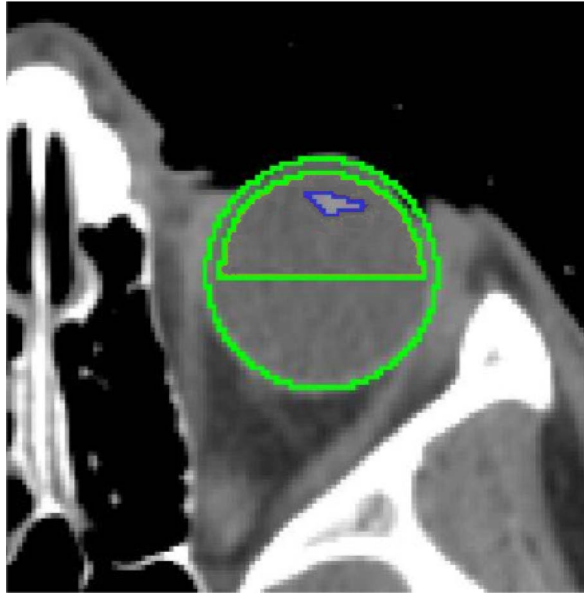


FIG. 4. Illustration of lens search area.

V.B. Segmentation of the lenses

The lens is approximated with an ellipsoid in the eyeball. To find its center the frontal hemisphere of the eyeball is thresholded, as the lens appears with definitely higher density than the other inner parts of the eyeball. The threshold is estimated on the basis of the histogram of the eyeball to select the brightest 3 percentile of the points. The center of the ellipsoid is chosen to be the centroid of the largest connected thresholded region (see Fig. 4). The size of the ellipsoid is given by constant ratios between the extents of the lens and the eyeball (based on anatomy). As the position of the lens depends on the viewing direction of the patient, the ellipsoid must usually be rotated with angle ϕ around the z axis and θ around the x axis

$$\phi = \arctan \frac{x_e - x_l}{y_l - y_e}, \quad (3)$$

$$\theta = \arctan \frac{z_l - z_e}{y_l - y_e}, \quad (4)$$

where $\mathbf{P}_e = (x_e, y_e, z_e)$ and $\mathbf{P}_l = (x_l, y_l, z_l)$ are the center of the eyeball and the lens.

V.C. Segmentation of the optic nerves

The segmentation of the optic nerves is the most difficult task because of their location and intensities. The third seed point is used to determine the optic nerves and the chiasm. The anterior part of the nerve is approximated using a cone and a cylinder, where the cone is tangent to the eyeball and the cylinder is positioned to enclose the optic canal (see Fig. 5). The anterior and posterior parts of the nerve are segmented separately. The anterior part is segmented as follows:

1. Fitting the cone
2. Fitting the cylinder

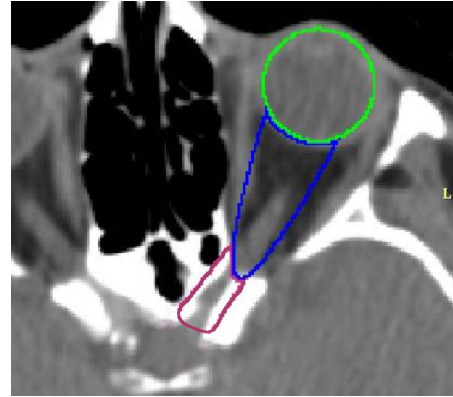


FIG. 5. Approximation of the optic nerve with a fitted cone and cylinder.

3. Approximate the anterior part of the nerve
4. Obtain the skeleton of the connected region
5. Reconstruct the anterior part of optic nerve from the skeleton

V.C.1. Fitting the cone

The fitting of the cone is illustrated in Fig. 6. The posterior point of the eyeball (denoted P) serves as the starting point for two scanning half lines (a and b). The first bone pixel found along the anterior-posterior scan-line a is denoted A , and B denotes the first bone pixel found along the scan-line b from

Algorithm 2 Approximate the anterior part of the optic nerve

```

1: Fit() //fit an ellipse on the selected coronal slice
2: Patch() //the thresholded region on the selected coronal slice
3: Next() //the index of the next slice according to the direction of
  propagation
4: Bridge() //connect two regions along the shortest voxel path
5:
6: StartSlice := G; EndSlice := D; reverse := false
7: fittedEllipse := Fit(StartSlice)
8: i := StartSlice
9: repeat
10:  i := Next(i)
11:  if fittedEllipse ∩ Patch(i) = ∅ then
12:    if reverse = false then
13:      StartSlice := EndSlice; EndSlice := i; reverse := true
14:      fittedEllipse := Fit(StartSlice)
15:    else
16:      Bridge(i, EndSlice)
17:      break //Go to 23
18:    end if
19:  else
20:    fittedEllipse := Fit(i)
21:  end if
22: until i = EndSlice
23: if i ≠ P then
24:   StartSlice := G; EndSlice := P; reverse := false
25:   Go to 7
26: end if

```

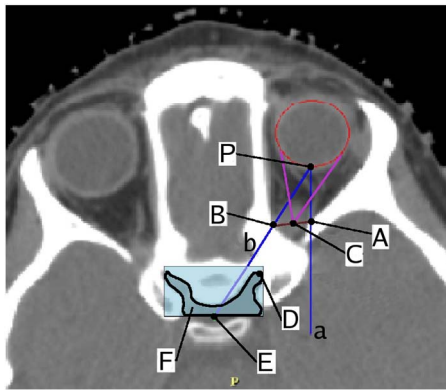


FIG. 6. Searching the apex of the cone. See text for details.

P to the chiasm seed point E . The midpoint C of the section AB is chosen as the apex of the cone.

V.C.2. Fitting the cylinder

The anterior end point of the cylinder is the apex C of the cone. A fixed size rectangle is attached to the chiasm seed point E (see shaded rectangle in Fig. 6). This region is thresholded to separate nerve tissue from bone and the largest connected nerve tissue component F is selected. The point of F closest to C is chosen as the posterior end-point D of the cylinder. The radius of the cylinder is fixed at 3 mm, which is an experimental value in agreement with the anatomy.

V.C.3. Approximate the anterior part of the nerve

Threshold the search region (the union of the cone and the cylinder) by the nerve intensity threshold. Let G be the centroid of the thresholded nerve region (see Fig. 6). Construct a connected region between D and P points by fitting ellipses in the coronal slices with Algorithm 2. An ellipse is initialized within the bounding rectangle of the thresholded region on the selected slice; its small and large axis are varied between 2 and 5 mm to find the parameters where the ellipse contains the least number of non-nerve voxels. The propagation of fitted ellipse is started from G to D first, then from G to P [see (a) in Fig. 7]. If the propagated shape does not intersect the thresholded nerve region on the current slice, the propagation is restarted from the end point D [see (b)

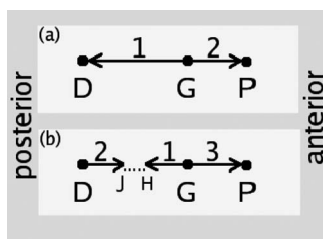


FIG. 7. Direction of ellipse propagation for the nerve approximation phases. See the text and Algorithm 2 for explanation.

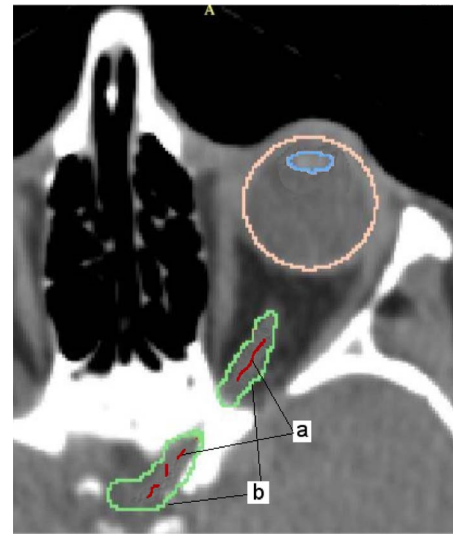


FIG. 8. The result of the masking procedure (labeled with b). The skeleton (the curve labeled with a) is continuous in 3D between the seed points.

Fig. 7] backwards and the two obtained segments are connected by a set of voxels along the shortest connection path between H and J .

V.C.4. Obtain the skeleton of the connected region

In Step 4 above a special 3D shrinking algorithm—derived from a sequential thinning algorithm⁷—is used to get the skeleton of the connected region (which is a rough approximation of the nerve volume) while keeping the end points (D and P).

V.C.5. Reconstruct the anterior part of optic nerve from the skeleton

For the reconstruction of the nerve volume from the skeleton, a special mask is defined in which each element is associated with a lower and an upper threshold for the attenuation (HU) related to the nerve tissue voxels. This mask is aligned at each point of the skeleton and voxels are included in the reconstructed volume if their intensity falls between the thresholds specified by the mask at that point. The threshold range at the mask elements gets tighter with increasing distance from the center point. Thus, close to the skeleton every point is included in the reconstructed volume, but at about 3 mm away only points with attenuation values corresponding definitely to the nerve are included, and beyond that no points are included at all. Thus, the inclusion of too much muscle tissue touching the nerve can be avoided while a thinner thread will still be kept in the bony canal (even if the canal appears blocked, i.e., the passage could not be seen on some coronal slices). The result of this masking procedure (the region labeled b in Fig. 8) will be considered as the segmented anterior part of optic nerve.

The determination of the posterior part is related to the optic chiasm segmentation (see Sec. V D).



FIG. 9. The shape of the optic chiasm in a photo.

V.D. Segmentation of the optic chiasm

Accurate outlining of this object is very difficult, because its intensity values cannot be easily separated from its environment. It is modeled with a 3D predefined shape (see Fig. 9) that is positioned around the third seed point and helps to distinguish between the chiasm and the posterior part of the nerve. The shape was determined as an average of a plurality of optic chiasms that were manually outlined by experts. The segmentation is the following:

1. Position the predefined model by overlaying its centroid with the chiasm seed point, and uniformly scaling it within a certain range such that the number of covered bone voxels are minimal.
2. Get the connected nerve region around the chiasm seed point (denoted F in Fig. 6), which contains the posterior end-point D of the cylinder.
3. Determine the skeleton of the connected region between the chiasm seed point and D using the same algorithm as for the anterior part.
4. Perform the same masking procedure to reconstruct the nerve volume as in case of the anterior part.
5. Classify the voxels based on a distance limit (which comes from the positioned model) into two groups: optic chiasm and posterior part of the optic nerve.

VI. EVALUATION METHOD

We evaluated our method on a set of 41 head CT studies randomly selected from a database of images acquired at different institutions for various (mostly diagnosis) purposes and not specifically for segmenting the eye and optic nerve regions.

The orientation of the image volume was head-first supine in all cases. Acquisition protocols, however, were quite different from study to study. All 3D datasets contained a stack of reconstructed two-dimensional axial slices of size 512×512 pixels with various sizes between 0.4 and 0.98 mm. The slice thickness varied between 0.625 and 2.5 mm among the datasets.

We used the measurements described by Udupa *et al.*⁸ to measure the precision of our algorithm with intra-operator repeatability, inter-operator reproducibility. The accuracy was tested with the simultaneous truth and performance level

estimation (STAPLE) method published by Warfield *et al.*⁹ We got qualitative measurements from the statistically processed opinions of clinicians.

VI.A. Accuracy

We started the evaluation by creating manual ground truth but after having a few manual segmentations, we found that it is not only time consuming but, more importantly, the results are not reliable. The segmentations show a large variation because of the small size and pose of the organs compared to the image resolution and slice orientation. For example, the optic nerve could be detected well on particular oblique slices, but clinicians use axial slices for diagnosis and, therefore, for segmentation as well. We had cases where the intersection of two manual segmentations of the optic chiasm in the same image volume was empty. Therefore, we decided not to create a gold standard. We used the STAPLE algorithm as an alternative solution to get information about accuracy compared to an estimated gold standard. The algorithm considers a collection of segmentations and computes a probabilistic estimate of the true segmentation and a measure of the performance level represented by each segmentation. It produced sensitivity (true positive fraction) and specificity (true negative fraction) measurements. The eyeballs and the lenses are handled separately in every step of the evaluation.

VI.B. Efficiency

Efficiency shows the practical viability of the method. Two factors are considered: computational time and the amount of human interaction required to complete the segmentation.

The computational (running) time is highly dependent on what type of hardware the program is running on. Simply by switching CPU architecture or CPU clock frequency, wall clock running time may change substantially. Therefore, a fixed test environment was defined and the running times were measured on the same hardware that the clinicians use in the everyday practice. The experiments were performed on HP workstation xw8200 with 2 GB memory and Intel Xeon 3400 processor using Fedora Core 3 operating system.

Evaluating human interaction is quite a complex problem on its own, so we asked the operators to rate the simplicity/difficulty of seed point selection as part of the evaluation questionnaire.

VI.C. Precision

Intra- and inter-operator precision were measured as follows. Let I_1 and I_2 denote the two binary segmented volumes and $|\cdot|$ the set cardinal operator. The similarity measure is defined as

$$M = \frac{|I_1 \cap I_2|}{|I_1 \cup I_2|} \cdot 100\% , \quad (5)$$

that is, the volume of the intersection of the two segmentations (i.e., the number of voxels that were segmented in both

TABLE I. The questionnaire and the ratings (expressed in %).

	Question	Good	Acceptable	Bad
1	Rate the quality of the image to be segmented -presence of noise or artifacts.	89.27	6.34	4.39
2	Rate separation from surrounding tissues.	85.37	12.68	1.95
3	Rate detection of eyeballs.	95.12	3.90	0.98
4	Rate detection of optic nerves.	51.22	38.05	10.73
5	Rate the computations speed.	98.05	1.95	0.00
	Question	Yes	Almost	No
6	Can the starting seed point(s) be easily given? (almost=yes, except the chiasm seed)	86.34	9.76	3.90
7	Can the segmented eyes and optic nerves be used as it is, or after a slight manual editing? (almost=yes, with slight editing)	66.83	27.32	5.85

I_1 and I_2) normalized by the volume of the union of the two (i.e., the number of voxels that were segmented in at least one of I_1 and I_2) expressed in percent.

For intra-operator precision measurements, one operator (A) performed the same segmentation task three times (denoted by A_1, A_2, A_3). For each corresponding segmentation pair ($A_1-A_2, A_1-A_3, A_2-A_3$), the M value is computed by substituting the two outputs in a pair for I_1 and I_2 . This is repeated for each study and the mean and standard deviation of the normalized overlap is computed among all tasks (three times the number of studies) to provide an overall reproducibility measure.

For inter-operator precision, three operators (A, B, C) performed the same segmentation task. The M value for each corresponding segmentation pair ($A-B, A-C, B-C$), and the overall reproducibility measure are computed analogously to the intra-operator case, but here, substituting the segmentation output by two different operators for I_1 and I_2 , instead of two outputs by the same operator.

VI.D. User opinions

It is very important to know the opinion of the clinician about the segmentation algorithm. It influences the usage of the method in the clinical practice. Therefore, after the automatic process created a segmentation using their seed points, the clinicians were asked to fill out a questionnaire (see Table I) and judge their “own” results after the semiautomatic segmentation for each study.

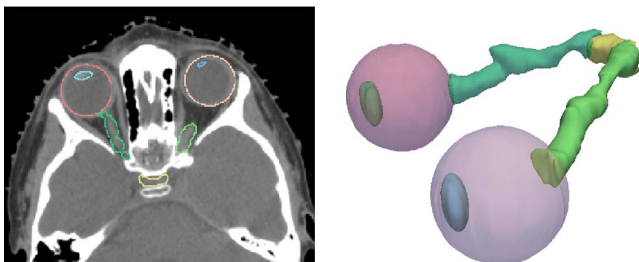


FIG. 10. The segmented organs (eyeballs, lenses, optic nerves, and chiasm) on a CT slice and their 3D model.

VII. RESULTS AND DISCUSSION

Figure 10 illustrates the final results of our algorithm on a 2D axial slice and in 3D with surface rendering. The evaluation shows both the strengths and weaknesses of the algorithm. Table I shows the statistics of the clinicians’ judgments in connection with usability and speed.

VII.A. Accuracy

The results of the STAPLE method (see Table II) show that the specificity of the method meets the requirements, for which there is no large over-segmented region. The sensitivity of the eyeball and lens segmentation is very good. In case of the nerve and optic chiasm we found that they are sensitive for the selected seed points, therefore, their accuracy is often below the expectations.

VII.B. Efficiency

The work flow permits segmenting the organs one by one and simultaneously as well. Certain organs can be re-segmented by repositioning the relevant seed points. The running time (see Sec. VI B) of the segmentation for the seven structure is within 5–6 s in one CT image volume (manual segmentation is about 20–25 min). The wall clock time (which includes the time for seed point selection) was not measured, but the users commented on this factor also on the questionnaire (see Table I). The operators deemed the running time good and the seed point selection easy. The

TABLE II. Accuracy estimated with STAPLE (mean \pm std. dev. of sensitivity and specificity in %).

Organ	Sensitivity	Specificity
Left eyeball	97.41 \pm 4.35	98.42 \pm 1.97
Left lens	97.57 \pm 4.22	98.41 \pm 2.36
Right eyeball	98.00 \pm 3.00	97.90 \pm 3.00
Right lens	98.04 \pm 2.91	98.13 \pm 2.61
Left nerve	75.76 \pm 18.14	99.07 \pm 0.88
Right nerve	77.82 \pm 14.63	99.04 \pm 0.86
Optic chiasm	65.20 \pm 28.47	93.50 \pm 6.98

TABLE III. Intra-operator repeatability (mean \pm std. dev., worst and best cases, expressed in %).

Organ	A_1-A_2	A_1-A_3	A_2-A_3	Overall	Worst case	Best case
Left eyeball	92.98 \pm 8.75	93.96 \pm 6.74	93.53 \pm 6.10	93.49 \pm 7.20	63.17	100.00
Left lens	92.87 \pm 9.09	94.44 \pm 6.85	93.16 \pm 6.02	93.49 \pm 7.32	60.49	100.00
Right eyeball	94.78 \pm 5.83	92.64 \pm 6.56	93.80 \pm 7.90	93.74 \pm 6.76	60.21	100.00
Right lens	94.79 \pm 6.71	93.18 \pm 6.76	93.76 \pm 8.59	93.91 \pm 7.35	54.22	100.00
Left nerve	65.15 \pm 25.87	64.16 \pm 23.57	62.49 \pm 21.82	63.93 \pm 23.75	18.17	100.00
Right nerve	70.11 \pm 18.76	71.63 \pm 17.29	70.96 \pm 18.58	70.90 \pm 18.21	29.36	99.86
Optic chiasm	57.45 \pm 31.10	53.56 \pm 30.46	52.46 \pm 30.48	54.49 \pm 30.68	0.00	100.00

selection of the seed points in the eyeballs is instantaneous and the third seed point can also be selected in a few seconds depending on the image quality and the experience of the user.

VII.C. Precision

The intra- and inter-operator reproducibility results are shown in Tables III and IV. The quality of the image to be segmented, that is, the presence of noise or artifacts, were mostly good, but the resolution of the images was different.

The precision of the segmentation of the eyeball and the lenses is above 90%, which means the eyeball and lens segmentation is not sensitive to the selection of (reasonable) seed points. These segmented structures can be used without manual editing. A small error is introduced by the spherical model for the eyeball, but it mostly cannot be realized or it is compensated with a margin during the therapy planning.

The repeatability and reproducibility of the optic nerve and chiasm segmentation are below our expectations, because it is sensitive to the positioning of the third seed point. Our experiences showed that detection of the optic chiasm (in which the third seed point should be positioned) is rather difficult. In a test two radiologists segmented the chiasm manually, and at the comparison the intersection of the two results was empty in the same image volume. Our test image database was created from images, which were acquired for different purposes, therefore the slices' thickness changes between 0.625 and 2.5 mm. If the user selects the third seed point with one or two slices higher or lower, the result can be very different because of the small size of the target organs (see Fig. 11). However, our experiences also show that, with some practice, the positioning of the chiasm seed point can be improved, which also improves the segmentation output.

During the investigation of the best and worst cases we found that the results are very good if the slice thickness is less than or equal to 1 mm. The precision is getting worse as the slice thickness is increasing. The poor contrast and lots of noise caused the worst case in the eyeball and lens segmentation results.

If the segmentation is not correct, it can usually be improved by a little manual editing, and even in such cases, the whole process (automatic part+manual editing) is faster than fully manual outlining. Manual segmentation is usually performed on axial slices, but because the image slices are not in alignment with the optic nerve and the slice thickness is also comparable to that of the nerve, the nerve may not show as disconnected pieces on the axial slice images, sometimes it may even be disconnected in the 3D discrete volume, even though it is clearly connected in the 3D anatomical space. When the nerve is disconnected on the axial slices the automatic segmentation can use the coronal slices for find connecting shortest paths between those nerve sections. The easy-to-use workflow and the short running time (1–2 s per structure) make it possible to re-segment one or all structures with modified seed points. The result can be corrected with two or three trials in case of the nerve. The clinicians mostly use this solution to get the appropriate result.

Our algorithm works well on children's data as well, because the model is created on the fly and is scaled appropriately with the help of the user given seed points.

VIII. CONCLUSION

The test results and the opinions of the clinicians show that our segmentation method (as is, or followed by a little manual editing) can be used in the clinical practice. Its efficiency allows speeding up radiotherapy treatment planning.

TABLE IV. Inter-operator reproducibility (mean \pm std. dev., worst and best cases, expressed in %).

Organ	$A-B$	$A-C$	$B-C$	Overall	Worst case	Best case
Left eyeball	93.82 \pm 6.23	93.41 \pm 6.75	92.19 \pm 8.16	93.14 \pm 7.05	62.54	99.86
Left lens	94.54 \pm 4.77	93.12 \pm 7.75	92.76 \pm 8.09	93.47 \pm 6.87	60.74	100.00
Right eyeball	93.77 \pm 5.83	93.13 \pm 6.67	93.00 \pm 6.18	93.30 \pm 6.23	69.82	99.74
Right lens	94.82 \pm 4.44	94.23 \pm 5.45	93.44 \pm 5.31	94.16 \pm 5.07	77.61	100.00
Left nerve	36.06 \pm 18.87	41.83 \pm 23.22	56.79 \pm 25.09	44.89 \pm 22.39	10.41	99.83
Right nerve	34.90 \pm 18.72	40.48 \pm 23.22	60.19 \pm 19.96	45.19 \pm 20.78	12.51	97.41
Optic chiasm	12.27 \pm 17.81	18.90 \pm 25.55	48.88 \pm 32.01	26.68 \pm 25.13	0.00	100.00

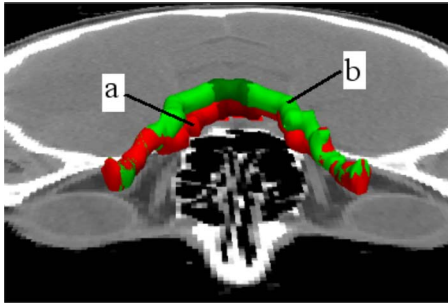


FIG. 11. Good (labeled with a) and bad (labeled with b) result of the nerve segmentation depending on the location of the third (chiasm) seed point (perspective view).

The presented method is integrated with the Advantage Sim MD¹⁰ radiotherapy planning software of GE Healthcare and used in the daily routine. The experiences show that the usability of the method can be further improved with some correction of the optic nerve and chiasm detection. We plan an automatic seed point adjustment based on the detection of the sella turcica and analysis of the expected result. The position of the optic nerve changes depending on the position of the seed point. If the seed is selected too high or low, the nerve will run out from the optic canal and crosses the bony structures of the orbit. The seed point can be repositioned based on the detection of this crossing.

ACKNOWLEDGMENT

The authors thank Csaba Pintér for coding some of the algorithms and for constructive feedback.

^{a)}Electronic mail: gyorgy.bekes@ge.com

¹B. Dobler and R. Bendl, "Precise modeling of the eye for proton therapy of intra-ocular tumours," *Phys. Med. Biol.* **47**, 593–613 (2002).

²A. S. A. Souza and E. E. S. Ruiz, "Fast and accurate detection of extraocular muscle borders using mathematical morphology," in *Proceeding of the 22nd Annual International Conference of IEEE*, Vol. 3, pp. 1779–1782 (unpublished).

³M. R. Kaus, V. Pekar, R. McNutt, J. Shoenbill, M. Moreau, D. H. Robinson, "Model-based segmentation for treatment planning with Pinnacle3," http://www.heartstream.com/main/products/ros/assets/docs/white_papers/453598304371_A.pdf

⁴P. F. D'Haese, V. Duay, R. Li, A. d'Aische, T. E. Merchant, A. J. Cmelak, E. F. Donnelly, K. J. Niermann, B. Macq, and B. M. Dawant, "Automatic segmentation of brain structures for radiation therapy planning," *Proc. SPIE* **5032**, 517–526 (2003).

⁵J. E. Cates, R. T. Whitaker, and G. M. Jones, "Case study: An evaluation of user-assisted hierarchical watershed segmentation," *Med. Image Anal.* **9**, 566–578 (2005).

⁶J. D. Foley, A. van Dam, S. K. Feiner, and J. F. Hughes, *Computer Graphics: Principles and Practice*, Addison-Wesley Longman Publishing Co., Inc. (1990).

⁷K. Palagyi, E. Sorantin, Cs. Halmai, and A. Kuba, "A sequential 3D thinning algorithm and its medical applications," in the *Proceeding of 17th Int. Cong. Information Processing in Medical Imaging*, pp. 409–415 (2001).

⁸J. K. Udupa, V. R. LaBlanc, H. Schmid, C. Imielinska, P. K. Saha, G. J. Grevera, Y. Zhuge, L. M. Currie, P. Molholt, and Y. Jin, "Methodology for evaluating image segmentation algorithms," *Proc. SPIE* **4684**, 266–277 (2002).

⁹K. Warfield, K. H. Zou, and W. M. Wells, "Simultaneous truth and performance level estimation (STAPLE): An algorithm for the validation of image segmentation," in *Medical Imaging*, *IEEE Trans.* **23**(7), 903–921 (2004).

¹⁰General Electric-Advantage Sim MD, <http://www.gehealthcare.com/usen/oncology/advsim.html>